Corrosion Science 152 (2019) 249–260

Contents lists available at ScienceDirect

Corrosion Science

journal homepage: www.elsevier.com/locate/corsci

Corrosion of uranium in liquid water under vacuum contained conditions. Part 1: The initial binary U + $H_2O_{(l)}$ system

A. Banos*, K.R. Hallam, T.B. Scott

University of Bristol, Interface Analysis Centre, School of Physics, HH Wills Physics Laboratory, Tyndall Avenue, Bristol, BS8 1TL, United Kingdom

ARTICLE INFO

Keywords:
Uranium
Water corrosion
Bulk-UH_3
Threshold pressure
FIB

ABSTRACT

The reaction of unirradiated-U with liquid water was investigated under initial vacuum-contained conditions. Ten samples were examined at varying temperatures and reaction times. Post-corrosion examination of the surfaces was conducted using FIB, SIMS and XRD. Measurements of the reacting water pH and degassing of the samples was conducted after the reaction was stopped. From the analyses, it was concluded that bulk-UH_3 formation occurred on the majority of the samples. It is suggested that UH_3 formation was facilitated by a critical 'threshold' headspace pressure ~0.5bar over which pressure deficiency is observed in the free headspace.

1. Introduction

The Sellafield legacy ponds and silos are plants used for the interim storage of untreated waste associated with first generation reprocessing of early military and commercial activities [1,2]. Intermediate level waste (ILW), comprised of radioactive sludge and uranium-contaminated materials like Magnox cladding, etc. have been accumulated in these plants for over six decades to keep them safely isolated from the environment [1,3]. In the early days of nuclear power, there was no in depth consideration for further treatment, repackaging or disposal of this material. Only later, when the challenges of storing such reactive metals was better understood, were plants designed to retrieve and process these wastes constructed [2–4].

The initial concept of storing these wastes under the cover of water has since proven to be problematic in some respects related to the long-term presence of uranium metal in a water-rich environment. The oxidative reaction of water with uranium produces uranium dioxide (UO_2), and H_2 gas. If this arising gas is confined in high concentrations it may react with any residual metallic uranium to produce uranium hydride (UH_3) (Eqs. (1) and (2)). Uranium hydride may behave pyrophorically under sudden exposure to air and under certain conditions (large quantity and high surface area). Thus, its formation is considered as an unwanted corrosion event. There has been an ongoing controversy between different research groups on whether the solid corrosion products arising will contain UH_3 [5–17] or not [18–21], in addition to UO_2, and if so, how much is likely to be present and in what distribution. It is believed that a number of parameters affect the development (or not) of UH_3 during wet corrosion. If in an enclosed/sealed system, H_2 generated from the oxidation of metals may remain trapped in the immediate vicinity and build-up in pressure as corrosion progresses. After a period of time, this gas may locally reach a critical concentration to undergo direct reaction with any uranium metal present [5,9,16]. In a continuous flow system, the carrier gas sweeps away the generated H_2; thus UH_3 formation may not be observed because the critical gas pressure required to initiate a bulk reaction is never achieved [7,19]. The physical state of water (solid, liquid, vapour), alongside the temperature could potentially play a key role in determining whether UH_3 will be produced [5]. Frank and Roebuck [5] observed higher amount of hydride formation when uranium was corroded under saturated water vapour conditions to that under immersed conditions for the same temperature [5]. It is also expected that oxidation occurring in temperature regimes close to where maximum hydriding rates are observed (160–270 °C) would be most likely to promote UH_3 formation, if hydrogen and/or water vapour pressure is adequate [9,22].The abundance of oxidising entities such as water, oxygen and/or hydrogen is very important and affects the existence (or not) of UH_3 in the product, while also affecting the kinetics of water corrosion [23]. Uranium hydride has been verified as either a final reaction product of water oxidation of metallic uranium [5,6,13–16] or as an intermediate [8,9,11,17]. The latter case is believed to enhance the reactivity of the metal [8,10,11].

$$U_{(s)} + 2H_2O_{(l)} \rightarrow UO_{2(s)} + 2H_{2(g)} \quad (1)$$

$$2U_{(s)} + 3H_{2(g)} \rightarrow 2UH_{3(s)} \quad (2)$$

Nuclear storage ponds represent obvious open-air systems whereby

* Corresponding author.
E-mail address: antonis.banos@bristol.ac.uk (A. Banos).

https://doi.org/10.1016/j.corsci.2019.02.017
Received 18 September 2018; Received in revised form 13 February 2019; Accepted 14 February 2019
Available online 12 March 2019

entrapment of hydrogen gas is highly unlikely. By comparison, storage silos might be expected to behave a little less predictably due to the possibility of there being local physical traps for hydrogen and possibility that dissolved oxygen may be depleted due to poor contact with air. Hydrogen arising from uranium oxidation, but more predominantly from the oxidation of other metals like Magnox cladding, steel, aluminium, etc., is assumed to mostly diffuse out and liberated into the air. However, and due to the very complex disposal of the material in the silos, and to a much less extent the ponds, there is a potential for trapping of gaseous oxidation products that are in close proximity to uranium metal. The existence of sludge-entrapped hydrogen bubbles in the ponds has been recently documented in Sellafield [24]. If any such 'pocket' of hydrogen coincides with 'uranium-rich' areas, then UH_3 formation will occur, if the threshold hydrogen pressure for hydride formation is achieved. UH_3, if produced, is regarded as an unwanted corrosion product due to its highly unstable and pyrophoric nature in air [25,26]. This fact raises safety and technical concerns when designing processes for safe retrieval, handling and repackaging of such legacy materials for onwards long-term storage in new facilities. On this basis, it is critical, prior to retrieval, for the physiochemical state of the waste to be directly characterised (which is difficult due to technical, logistical and access restrictions) or adequately predicted (which is the operational case). Understanding the extent of the ongoing corrosion is also very important, especially during transitioning from one storage environment to another, where temporal disturbance of the waste (chemical or mechanical) may induce significantly different corrosion conditions, compared to the conditions previously experienced.

In this paper, we attempted to simulate/mimic legacy waste storage conditions, by conducting a series of experiments whereby non-irradiated uranium was immersed in distilled water and left to oxidise, under initially evacuated headspace conditions, at different temperatures. In a very early work, Frank and Roebuck [5] corroded uranium in water under similar immersed and saturated conditions in an enclosed system and verified UH_3 production for both systems [5]. However, these experiments were conducted at high temperatures (260 °C) where UH_3 is favoured to form most rapidly, and are therefore not of direct relevance to the storage temperatures experienced by wastes at Sellafield. Draley et al. [6], working at a lower temperature (100 °C), also observed hydride formation at the metal-oxide interface, which was responsible for the disruption and lack of coherence of the growing surface oxide [6]. A later and more extensive work by Baker et al. [9] provided some guidelines for the reaction of uranium in liquid water in an enclosed system (but without headspace gas). They examined the system for a wide range of temperatures (35–240 °C) and concluded that UH_3 is produced as an intermediate product of wet oxidation, with UH_3 production further enhanced at high temperatures due to improved uranium-hydrogen kinetics [9]. In a very recent work, Martin et al. [27] used atom probe tomography (APT) to investigate the surface of uranium, corroding in an oxygen-free water vapour environment. Using deuterated water (D_2O) instead of H_2O, they confirmed the presence of a very thin but ubiquitous inter-layer hydride at the metal-oxide interface [27]. This hydride displayed a constant thickness (~5 nm) and worked as a reaction front, consuming the metal immediately at its base, concurrent to its upper surface being oxidised to form UO_2. In this current set of experiments, our aim was to examine the lower temperature reaction regime (25–70 °C) which has not previously been studied in detail and better represents the 'real' corrosion conditions of the legacy ponds and silos at Sellafield. Four temperatures (25 °C, 45 °C, 55 °C and 70 °C) were used in this work in an effort to encompass the temperature ranges reported for these environments in the literature.

2. Materials and experimental methods

2.1. Sample provenance and preparation

Non-irradiated Magnox uranium metal of the type used for Magnox reactors was used in this work. Characterisation of this material has been presented in previous publications [28–30]. The samples originated from Springfields Ltd. and were provided as metallic discs cut from a parent fuel rod. Through energy dispersive X-ray (EDX) analysis (not shown here), it was found that C, N, O, Al, Fe and Si were the main impurities in the metal, accompanying U. Uranium carbides, di-carbides and carbo-nitrides, which are the main embodiments of impurities in the metal, form during the fabrication process of the material owing to their much higher formation temperatures from a melt than uranium [31,32]. In the tested Magnox uranium, these inter-metallic compounds were almost homogeneously spread in the metal bulk as rectangular, cuboid, X-shaped or H-shaped features, with the average diameter ranging from 3 μm to as high as 18 μm [29,33]. The metal microstructure exhibited significant strain expressed in the form of slip planes and twin boundaries [29,33] and attributed to the fabrication process. 10 samples were prepared for the experiments, all originating from the same bar stock of non-irradiated natural uranium coupons. Table 1 integrates the initial parameters of the samples. The letter 'W' was used to designate the reactant (liquid water), the two middle numbers designated the temperature of the reaction and the ending letter denoting the reaction time, with 'S' and 'L' denoting short and long reaction times, respectively. A 'Long' reaction time was considered for experiments lasting > 900 h. For repeat samples corroded at the same conditions and for similar reaction times, an ending number was used to signify the number of the experimental run. Thus, for a sample that was reacted with water at 25 °C for a long-time period and was experimentally repeated, the denotation W25L was used for the first sample and W25L2 for the second.

2.2. Reactant water

Distilled water was used as a liquid reactant for uranium corrosion. The water was subjected to a three-stage freeze-vacuum-melt process to remove dissolved oxygen, thereby promoting anoxic reaction conditions.

2.3. Experimental apparatus

Fig. 1 shows an example reaction cell pot designed for the corrosion reactions of this work. The reaction cell pot body consisted of DN 63 CF tabulated flanges, and a half nipple, fully welded and sealed in the base end. The cell came in two different width sizes (63 mm and 135 mm). For each reaction pot, Swagelok ¼-inch stainless steel tubing with VCR fitting was modified to provide two free ends on the upper side of the cell. One end of the set-up was built to connect to a gas control rig, allowing evacuation of the gases from the working volume

Table 1
Preliminary parameters (weight & surface area) of the samples.

Sample	Weight (g)	Surface area (cm^2)
W25L	0.81	1.00
W25L2	1.35	1.25
W45S	4.98	3.63
W45L	1.97	1.94
W45L2	1.86	1.66
W55S	4.79	3.57
W55S2	1.92	1.82
W55L	2.12	2.03
W70S	5.35	3.81
W70S2	4.53	3.65

Fig. 1. Photographic image of the reaction cell set-up used for the long-term corrosion experiments.
Figure reproduced from [33].

($< 7 \times 10^{-6}$ mbar). A pressure-current transmitter with analogue output was fitted to the other side of the set-up to measure evolving pressure changes in the system. A ceramic crucible was used to contain the water and the immersed sample in each reaction cell. Lenton laboratory ovens (Welland series) were used to accommodate the reaction pots and maintain them at the desired temperature for the duration of each experiment.

2.4. Experimental method

Once the set-up was prepared, 4 ml of distilled water was added to each ceramic crucible using a syringe and the crucible was carefully positioned in the bottom of the pot. The cell was then sealed and the bottom half of the cell carefully immersed in a Dewar flask containing liquid nitrogen. After complete freezing of the water (~30 min after immersion), the working volume was evacuated to $< 2.5 \times 10^{-6}$ mbar, while N_2 immersion was maintained. When the desired vacuum was reached, the cell was isolated and disconnected from the rig, while being removed from the flask. After the ice had re-melted, accumulation of water vapour in the cell was readily detected (~31.6 mbar at 25 °C), and the freeze-evacuate-thaw cycle was repeated a further two times to drive off any dissolved gases e.g. oxygen or nitrogen. Immediately after the third evacuation, the cell was opened and the uranium sample was positioned on top of the ice-filled crucible. The cell was then sealed, re-immersed in liquid N_2 for the last time and evacuated to $< 1 \times 10^{-6}$ mbar. The whole set-up was then placed in the oven, to reach the desired corrosion temperature. Pressure changes were continuously logged from the very start of the process, using a 5-sec step. The reaction was eventually halted by withdrawing the set-up from the oven and disconnecting the logger. The reaction pot was immediately opened (in the lab) and the sample was carefully retrieved from the ceramic crucible. At this retrieval stage, samples that had been corroded for longer time periods and at higher temperatures exhibited a partial mass loss of the solid corrosion products, caused by spallation of significant accumulations of the corrosion products (Fig. 2). After drying in air for a couple of minutes, the sample was transferred to inert storage, stored in an Ar-filled glovebox, while awaiting post-corrosion examination and analysis. Partial mass loss from samples was considered inevitable through the retrieval and drying process.

2.5. Post reaction examination

Post examination of the reacted surfaces was used to identify the corrosion products of the reaction. Focused ion beam (FIB) milling was employed to physically inspect the surface and evaluate the morphology and characteristics of the solid reaction products, such as UO_2. It was also used to make deep trenches into the surface corrosion layers, in order to view the cross section and measure their thickness. X-ray diffraction (XRD) allowed identification of the solid corrosion products of the reactions, down to a certain depth. It is important here to note

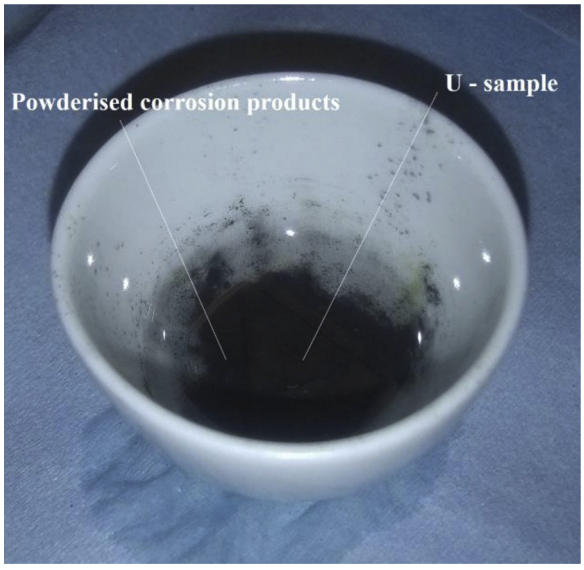

Fig. 2. Water-immersed, post-reacted uranium sample in a ceramic crucible. Flaked-off and powderised corrosion product is dispersed in the water. Partial mass loss was inevitable under retrieval and handling of the sample at this stage.
Figure reproduced from [33].

that due to limitations in the maximum energy of the X-ray source (~8 keV), the heavily oxidised surfaces could not be analysed down to the metal-oxide interface owing to attenuation of the X-rays in the outermost layers of the accumulated corrosion product. This restriction posed a challenge for confirming the existence (or not) of UH_3, forming and accumulating at the metal-oxide interface [34]. Secondary ion mass spectrometry (SIMS) was used as an alternative determination method for UH_3. SIMS allowed the relative abundance and distribution of chemical elements in the reacted surface to be determined by progressively etching down through the corrosion layer to the metal-oxide interface. The depth profile analysis was conducted at 25 keV, in positive Ga + ion mode, with 3 nA beam current (45° incident beam).

Temperature programmed desorption (TPD) combined with residual gas analysis (RGA) was employed to degas the samples and analyse the evolved gases. This allowed identification of the solid products of the reaction in a more indirect but quantitative manner. By understanding the temperature range for thermal decomposition of UH_3 it was possible to convert the pressure of evolved hydrogen gas to molar mass of precursor hydride.

2.6. Assumptions

Before proceeding to the results section, it is necessary to state and examine the validity of all the assumptions made for the analysis.

For the reaction rate determination methods, it was assumed that α-U is the only solid phase in the sample, prior to reaction. Such an assumption may be regarded as broad, especially for samples with high carbon content, where carbides and carbo-nitrides will unavoidably be present as a trace constituent. On such a sample, gaseous CH_4 and/ or NH_3 may be evolved during corrosion [31,35–38]. These contributions are regarded inconsiderable since α-U is the dominant phase in the system. Additionally, the results would be comparable between the different corroding conditions since the samples have the same provenance, and all calculations were conducted using the same assumptions.

The only solid and gaseous products of the U-oxidation reaction are $UO_{2(s)}$ and $H_{2(g)}$ generated as part of α-U oxidation (Eq. (1)). The exclusion of $UH_{3(s)}$ production through Eq. (2) was deliberate at this stage. For a system where UH_3 formation occurs, our measurements would lead to an underestimation of the corrosion rate, since oxidation-

generated H_2 would not be released in the gas phase, but would react with uranium to form UH_3. This scenario will be used later, to provide indirect evidence of UH_3 formation in the system based on observed changes in corrosion rate.

The arising hydrogen gas behaves as an ideal gas. For hydrogen, the standard deviation from the ideal gas law is less than 0.1% at room temperature and pressure [39] and, thus, this assumption is considered acceptable.

All samples have reached the linear stage of oxide development prior to participation in the experiment. This assumption was ensured by leaving the samples exposed to air for 45 min after final preparation to ensure formation of an oxide layer sufficiently thick that a linear corrosion rate had been established.

It is also assumed that no measurable reaction is taking place on the uranium surface during the time needed for water vapour saturation of the cell headspace to occur. A finite time period was required for every system to reach gas phase equilibrium at its set corrosion temperature. Any gas generation as part of the oxidation reaction for that time period is not included in our measurements. This short period is regarded inconsiderable when compared to the total reaction time of each system (100 s of hours).

There is negligible surface area change of the uranium sample over time with progressive corrosion. In practice, some surface area change will be observed as the sample is corroding and the metal is consumed. However, this effect will be comparable between samples.

The final assumption is that negligible change in the working headspace volume of the cell occurs during progressive sample volume expansion as corrosion progresses.

3. Results

Depending on early results from the initial experiments, it was decided to deliberately skip some of the analysis methods on some samples, to minimize cumulative damage. This was achieved by ensuring minimal intervention to the samples.

3.1. Reaction rate determination through gas generation

The reaction rate for each sample has been derived from the gas pressure changes in the system over time. Gas generation in the headspace, which was ascribed to H_2 (Eq. (1)) after water vapour pressure subtraction, was converted to milligrams of reacted U per unit area over time (mgU cm^{-2} h^{-1}) based on ideal gas law and stoichiometry of Eq. (1). Fig. 3 illustrates the wet corrosion progress, (in mgU cm^{-2}), over time, for W70S sample.

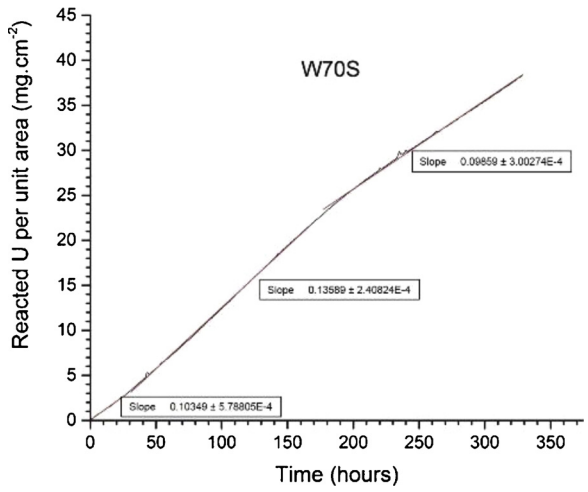

Fig. 3. Corrosion progress of uranium immersed in liquid water (in mgU.cm-2), over reaction time for a representative W70S sample.
Figure reproduced from [33].

Table 2 consolidates the various reaction rate regimes observed for all reaction conditions. All systems exhibited more than one rate regime with some of those exhibiting three distinct slopes (Table 2). The average reaction rate, shown in the last column of Table 2, was derived from averaging: (a) the average flux of the rate derived every hour; and (b) the rate, which was derived from the total cumulative value of U consumption, per unit area, divided by the total reaction time.

Fig. 3 displays a paradigm of the corrosion progress for the W70S sample over time. From the reaction rate line behaviour it can be observed that the rate initially switches to faster kinetics (~25 h) to eventually decelerate again more than half-way through the reaction period (~200 h).

Comparable rates have been documented in the literature for the 25 °C reaction regime, with the reported rates for aqueous corrosion at 21 °C ranging from 0.0075 to 0.0097 mgU cm^{-2} h^{-1} [40]. However, for the higher temperature regimes, the kinetics derived from this work are significantly slower in comparison to the literature. For example, Orman et al. [41] reports a rate of 0.071 mgU cm^{-2} h^{-1} for aqueous corrosion at 35 °C, which is as much as three times higher than the derived rate of this work, for reaction at ~45 °C. For 55 and 70 °C, the reported rates are as much as six times higher, in comparison to this work [9,41]. However, it should be mentioned that for all the other works the pressurised volume headspace was periodically relieved from the generated gas.

By plotting the values of the average reaction rates on an Arrhenius plot, the dependence of the reaction rate on the temperature and the energy of activation could be calculated. Fig. 4 illustrates the Arrhenius data plot for our corrosion of uranium in liquid water between 25–70 °C under contained conditions. Two samples (Fig. 4 – highlighted in red), representing W45L2 and W55S, showed unexpectedly low reaction rate. Thus, it was decided to generate the slope from linear regression of the Arrhenius plot by including and excluding these data points from the calculations.

Exclusion of these points from our calculations yielded the following equation:

$$Ln\ k = 15.394 - 6002.1/T \quad (3)$$

where k is the rate of the reaction in mgU cm^{-2} h^{-1} and T, the temperature in Kelvin. Since E_α/R is 6002.1 and with R being a constant value of 8.314 J $mole^{-1}$ K^{-1}, the activation energy was calculated 50 kJ mol^{-1}. Inclusion of these values to our calculations yielded an E_α/R of 5743 and an activation energy of 48 kJ mol^{-1}.

3.2. Reaction rate determination through oxide thickness calculation

An additional way of approximating the average corrosion rate for each experiment was to measure the average of multiple oxide thickness measurements across the surface and convert to mgU cm^{-2} h^{-1}. The thickness of the oxide was not uniform across the sample (Fig. 5a). Thus, multiple ion beam sections had to be made across the surface to better represent the oxide thickness for each sample. Observed gaps generated from delamination within the UO_2 layers were not included in the measurements to better approximate the oxide thickness value.

Fig. 5a and b illustrate representative cross-sectional views for the W45S and W70S2 samples, respectively. From physical observation of the cross-sectional views, the oxide appears to be extensively delaminated and increasingly porous and flakier with increasing reaction temperature and increasing reaction time. As the oxide grows in thickness, stress fields resulting from the volume mismatch between the oxide and metal, result in a loss of coherence and delamination cracking. From the cross-sections, it is unclear if UH_3 formation has taken place (or not), especially on the heavily oxidised samples. Considering the near identical mass density of the hydride and oxide, discernibility between the two through SEM was not expected to be possible.

Table 2
The reaction rate regimes derived from for each experimental condition.

Sample	Reaction time (hours)	Reaction rate 1st regime (mgU cm^{-2} h^{-1})	Reaction rate 2nd regime (mgU cm^{-2} h^{-1})	Reaction rate 3rd regime (mgU cm^{-2} h^{-1})	Average reaction rate (mgU cm^{-2} h^{-1})
W25L	1147.7	n/a	0.0204 ± 0.0006	0.005 ± 0.00005	0.0107
W25L2	978.4	n/a	0.0096 ± 0.00005	n/a	0.0086
W45S	126	0.0185 ± 00005	0.0274 ± 0.0002	n/a	0.0262
W45L	1621.6	0.0043 ± 0.0007	0.0137 ± 0.0004	0.0243 ± 0.00009	0.0215
W45L2	1046	n/a	0.0102 ± 0.0001	n/a	0.0098
W55S	345	0.0276 ± 0.0005	0.0149 ± 0.0001	0.0095 ± 0.00004	0.0148
W55S2	397.2	n/a	0.0791 ± 0.0001	n/a	0.0799
W55L	1618.2	n/a	0.0638 ± 0.00008	0.0517 ± 0.0003	0.0612
W70S	329	0.1035 ± 0.0006	0.1359 ± 0.0002	0.0986 ± 0.0003	0.1166
W70S2	436.3	0.0773 ± 0.0017	0.1084 ± 0.0019	0.0971 ± 0.001	0.0996

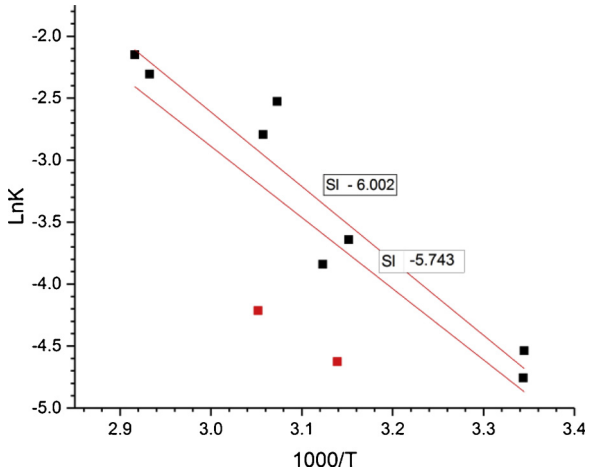

Fig. 4. Arrhenius data plot for corrosion of uranium with liquid water between 25–70 °C (saturated conditions). The points highlighted in red, representing W45L2 and W55S, were excluded from linear regression of the Arrhenius plot due to the unexpectedly low reaction rate recorded for these samples. Inclusion of these values to our measurements yielded an Eα = 48 kJ mol^{-1} (For interpretation of the references to colour in this figure legend, the reader is referred to the web version of this article).
Figure reproduced from [33].

Hydride formation in the system, if it occurs, is not necessarily uniform along the oxide-metal interface (spot-wise hydride formation is well reported [30,42,43]). During spot-wise hydride formation, the oxide immediately overlying any spot-growth would be vertically displaced. If a hydride growth were dissected during the cutting of a FIB trench, then due to the volume expansion, the ensuing oxide thickness measurements would provide an overestimation of the average oxide thickness. Thus, the derived reaction rate could be higher in comparison to the one derived from gas generation. In contrast, if by using the measured oxide thickness we derive slower reaction rates than those observed through gas generation, this could imply potential leaking of the cell whilst the reaction took place. Any major disparity observed between reaction rates determined via these two methods could provide an indirect, though not definitive, indication that UH_3 had formed on a sample.

Table 3 compares the reaction rates derived from the average of the oxide thickness measurements (FIB measurements) versus gas generation. From the results, it may be seen that only W25 L and W45S yielded similar rate values. The rate derived from direct oxide measurement on sample W25L2 was very low due to an observed detachment of the oxide from most parts of the surface. This resulted in underestimation of the rate for this sample. All the other samples yielded faster reaction rates derived through oxide thickness measurements in comparison to those derived from H_2 generation for the same system, with W55S yielding a rate almost three times higher than the one derived through gas generation. The difference between the obtained rates from the two methods could imply UH_3 formation. However, further analysis was required to strengthen any conclusion.

The generally higher reaction rate kinetics derived from oxide thickness measurements (FIB analysis) in comparison to H_2 generation analysis, implicates one or more of the following processes to be occurring in the reaction systems:

1 The generated H^+ (according to Eq. (1)) are not coupled and released to the headspace but remains trapped/dissolved in the water. This would result in underestimation of the rate derived from H_2 generation (as already confirmed from Table 3) and could be indicated by a change in the water pH.
2 The generated hydrogen is not released to the headspace or the reaction water but remains trapped in the immediate vicinity of the sample surface i.e. within physical traps (lattice, microstructural or pores) in the corrosion layer. This would also result in underestimation of the rate derived from H_2 generation.
3 The generated hydrogen (Eq. (1)) reacts with uranium to form UH_3 according to Eq. (2). This would result in reaction rate variance between the two methods (Table 3).

All above-mentioned processes will be examined in the following sections.

3.3. pH analysis of residual waters

If generated hydrogen remained dissolved in the water (in the form of H^+ ions), then it would be expected that the pH of the water would drop. The pH of the starting water after the final stage of the freeze-thaw vacuum purging process (prior to reaction) was measured and found to be 6.86 at 25.2 °C. The residual waters were measured immediately after each reaction was stopped.

Any potential difference in pH between the starting and residual water (pH drop) was then ascribed to hydrogen, originating from the oxidation reaction of uranium. By converting the pH difference to moles of H_2, the potential increase in cell H_2 pressure generation if the dissolved hydrogen were exsolved was calculated. Table 4 integrates results from the pH analysis. The pressure (Table 4 – column 7) was calculated by assuming that all excess H^+ coupled to form H_2 and could be released in the gas phase of the cell. In the analysis of Table 4, it was assumed that only the H^+ anions generated from oxidation contribute to the observed pH decrease. In practice, UO_2, which has low solubility in water, and small amounts of CO_2 originating from carbide phase oxidation will partly dissolve in the solution, causing the pH to decrease. Such overestimation was deliberately made, but regardless the quantities of dissolved hydrogen were negligible in all cases, attesting to the very limited solubility of hydrogen in water.

Residual versus starting pH values were measurably lower in all cases, but not significantly so. pH was generally lower at higher temperatures of reaction. This was likely partly attributable to increased

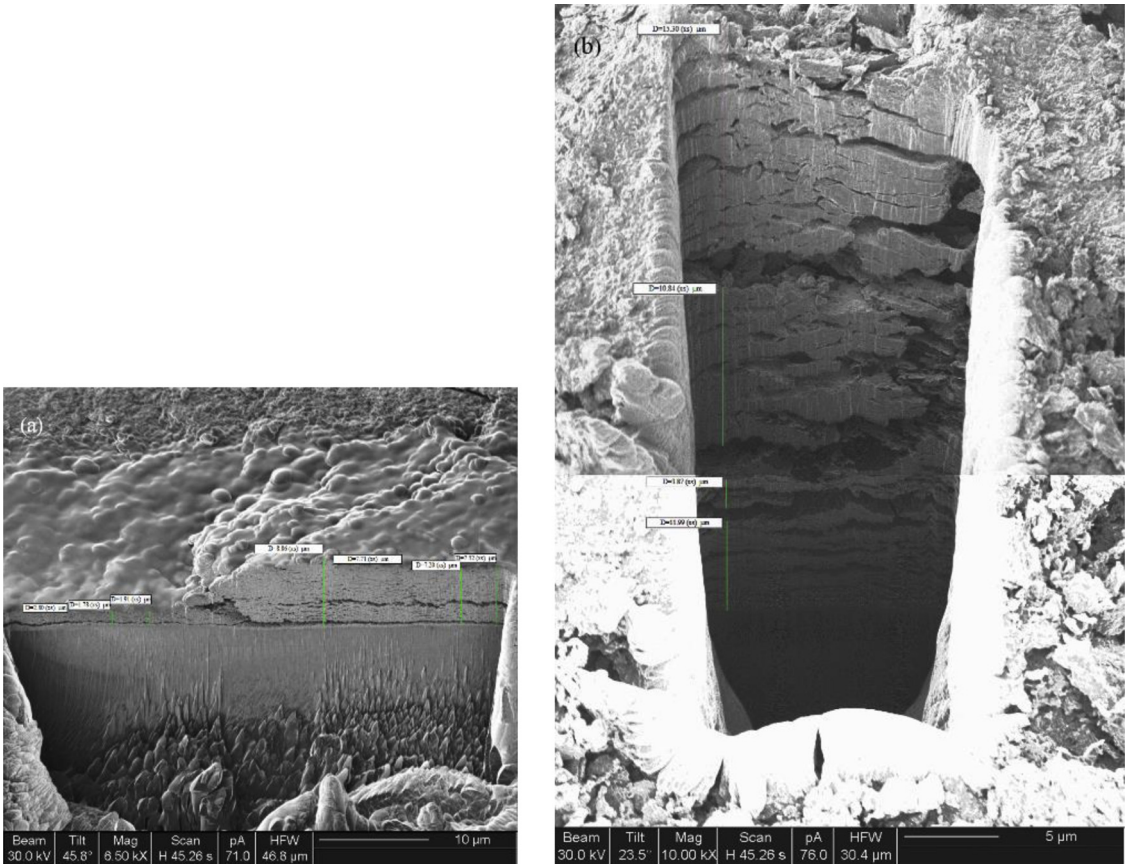

Fig. 5. Focused ion beam (FIB) milling images of representative cross-sectional views for: (a) W45S; (b) W70S2 sample. The measured thickness values represent only the part of the oxide which was adhered to surface. On (a) a single FIB image was needed to show the thickness of the oxide while on (b) (heavily corroded sample) two images were produced and stitched together to demonstrate the thickness of the layer.
Figure reproduced from [33].

dissolution of U into the water from the oxide.

Thus, it is determined for this specific experimental set-up, that hydrogen was not trapped in considerable quantities in the reactant water. The next step of the analysis would be to examine the residual uranium samples and verify if this hydrogen gas deficiency is attributable to one of the remaining processes (processes 2 and 3 presented above).

3.4. SIMS analysis

Through physical observation of the surface and by viewing the cross-section of each sample, information about the morphology of the reacted samples could be gained. However, no chemical identification of the corrosion products could be derived from this analysis. Mass spectrum analysis was initially conducted to identify the chemical species apparent in each sample. The existence of hydrides, hydroxides and carbide-nitride-oxygen clusters, along with uranium and uranium dioxide, were identified through mass spectrum analysis between 230 and 280 amu (Fig. 6). The formation of hydroxides on the outermost surfaces, through oxidation of uranium in liquid water and water vapour, has been documented before by Totemeier et al. [44].

SIMS depth profiling allowed examination of the corroded surface from the very top (gas-oxide interface) to the metal-oxide interface. Fig. 7 represents an illustrative mass ion depth profile for W70S sample. One potential process in the system, as mentioned above, would be for H_2 to remain entrapped in the sample, in the form of hydroxide compounds. Hydroxides were observed to form as part of wet corrosion (Fig. 6). However, to justify the H_2 pressure deficiency in the system, these phases should have significant determined thicknesses. By conducting multiple mass ion depth analysis profiles and examining the

Table 3
Corrosion layer thickness vs H_2 generation derived rate.

Sample	Average of corrosion layer thickness measurements (µm)	Reaction rate derived from average of corrosion layer thickness measurements (ascribed to UO_2) (mgU cm^{-2} h^{-1})	Reaction rate derived from H_2 generation (mgU cm^{-2} h^{-1})
W25L	12.76	0.0106	0.0107
W25L2	1.87	-[a]	0.0086
W45S	3.71	0.0285	0.0262
W45L	62.02	0.037	0.0215
W55S	14.81	0.0415	0.0148
W55L	166.02	0.0992	0.0612
W70S	91.76	0.2697	0.1166
W70S2	61.09	0.1354	0.0996

[a] W25L2 oxide flaked off leading to significantly smaller average thickness.

Table 4
Reaction water pH measurements and H_2 concentration calculation (as pressure increase if in the gas phase), for all samples of the binary system.

Sample	pH of water at average temperature of reaction[a]	pH of reactant water at average temperature of reaction	Difference in concentration of H^+ between original and reactant water (mole lt^{-1})[b]	Difference in H_2 in reactant water (mmol)[c]	Working/ reaction volume (cm^3)[d]	Pressure increase if excess H_2 diffused out to the gas phase (mbar)
W25L	6.85	Not measured	n/a	n/a	n/a	n/a
W25L2	6.85	6.13	5.98E-07	1.2E-06	84.81	0.00035
W45S	6.57	Not measured	n/a	n/a	n/a	n/a
W45L	6.53	6.00	6.98E-07	1.4E-06	84.77	0.00044
W45L2	6.55	6.18	3.87E-07	7.75E-07	84.80	0.00024
W55S	6.45	5.96	7.37E-07	1.47E-06	84.61	0.00047
W55S2	6.44	6.07	4.89E-07	9.78E-07	80.91	0.00033
W55L	6.45	6.12	4E-07	7.992E-07	84.76	0.00025
W70S	6.29	5.75	1.27E-06	2.54E-06	180.05	0.00,040
W70S2	6.30	6.00	5.08E-07	1.02E-06	84.62	0.00034

[a] pH at 25.2 °C, 6.86. Linear extrapolation to the temperature of reaction and, thus, approximate value.
[b] Volume of water = 4 ml.
[c] If all excess H^+ coupled to form H_2.
[d] Inconsiderable change in the working volume due to sample's volume expansion and liquid water consumption.

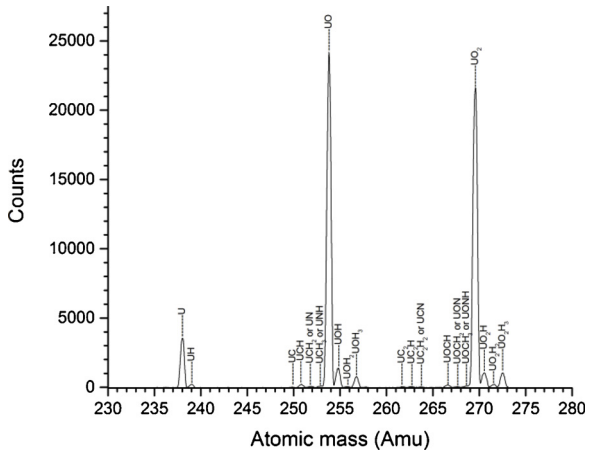

Fig. 6. Post-reaction mass spectrum analysis (230–280 amu) for sample W70S. Hydrides, hydroxides, carbide-nitride-oxygen clusters and oxides can be seen in the spectrum.
Figure reproduced from [33].

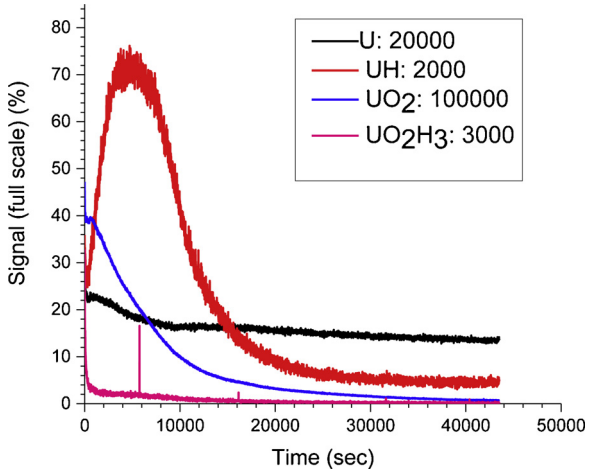

Fig. 7. Secondary ion mass spectrometry (SIMS) depth profile for W70S sample. The analysis was performed with a Ga + primary ion beam, 25 keV voltage, 3 nA beam current, and 45° angle of incidence.
Figure reproduced from [33].

profile behaviour of these hydroxides (such as UO_2H_3, etc.) it was found that these phases were only apparent very close to the outer layers of the oxide surface, at the gas-oxide interface. The limited abundance of these hydroxide phases could not justify the observed pressure deficit for H_2 in the system.

The final scenario that could justify the H_2 pressure deficit, or the overestimation of the oxide layer thickness (Table 3), is the existence of UH_3 in the sample. For a sputtered region containing a hydride, at or near the metal oxide interface, the ion-cluster signal representing the hydride phases should increase in intensity. At the metal-oxide interface, the UO_2 signal is expected to decrease, while the uranium signal should either stay constant or increase in value, however, not correlated with the UH signal. This would yield a ratio of UH/U which would start to increase in value when the upper end of the hydride is first sputtered; reach a maximum value near the centre of an assumed ellipsoid-shaped hydride and eventually decrease as the base of the hydride is sputtered.

For the majority of the reacted surfaces, SIMS analysis could not provide direct evidence of bulk-UH_3 formation at the metal-oxide interface. It is believed that such analysis was becoming much less reliable for heavily oxidised surfaces where deep trenches were made on loosely adhered corrosion product, leading to noisy mass ion depth profiles. Only the analyses on sample W70S yielded direct evidence for hydride formation (Fig. 7). For the samples other than W70S, hydride formation cannot be excluded by SIMS analysis, nor confirmed.

3.5. XRD analysis

Through FIB and SIMS analysis alone, it was not possible to directly determine if uranium hydride was commonly produced on the reacted surfaces. Reaction rate determination through oxide thickness measurements implied either a H_2 gas pressure deficit or UH_3 formation. By measuring the pH of the reactant water and conducting multiple mass ion depth profiles, it was possible to establish that only insignificant amounts of hydrogen might be accounted for as dissolved H^+ or in forming uranium hydroxide phases.

XRD was selected as a reliable way of determining if UH_3 has formed at the metal-oxide interface. However, this characterisation method was not initially selected as a primary characterisation tool due to the fact that our samples would react for long periods with water, leaving a significant thickness of accumulated corrosion products. The thick oxide covering could attenuate the X-rays to an extent where no information about the phases at or near the metal-oxide interface could be derived. For that reason, it was decided to perform the analysis on a limited number of samples which were deliberately reacted for a shorter time period. Four samples (W25L2, W45L2, W55S2 and W70S2) were analysed using XRD. Fig. 8a–d show the XRD patterns for each sample.

Samples W45L2 and W70S2 exhibited four peaks at approximately 26.87°, 30.12°, 49.53° and 51.54° 2-theta (θ) ascribed to the β-UH_3

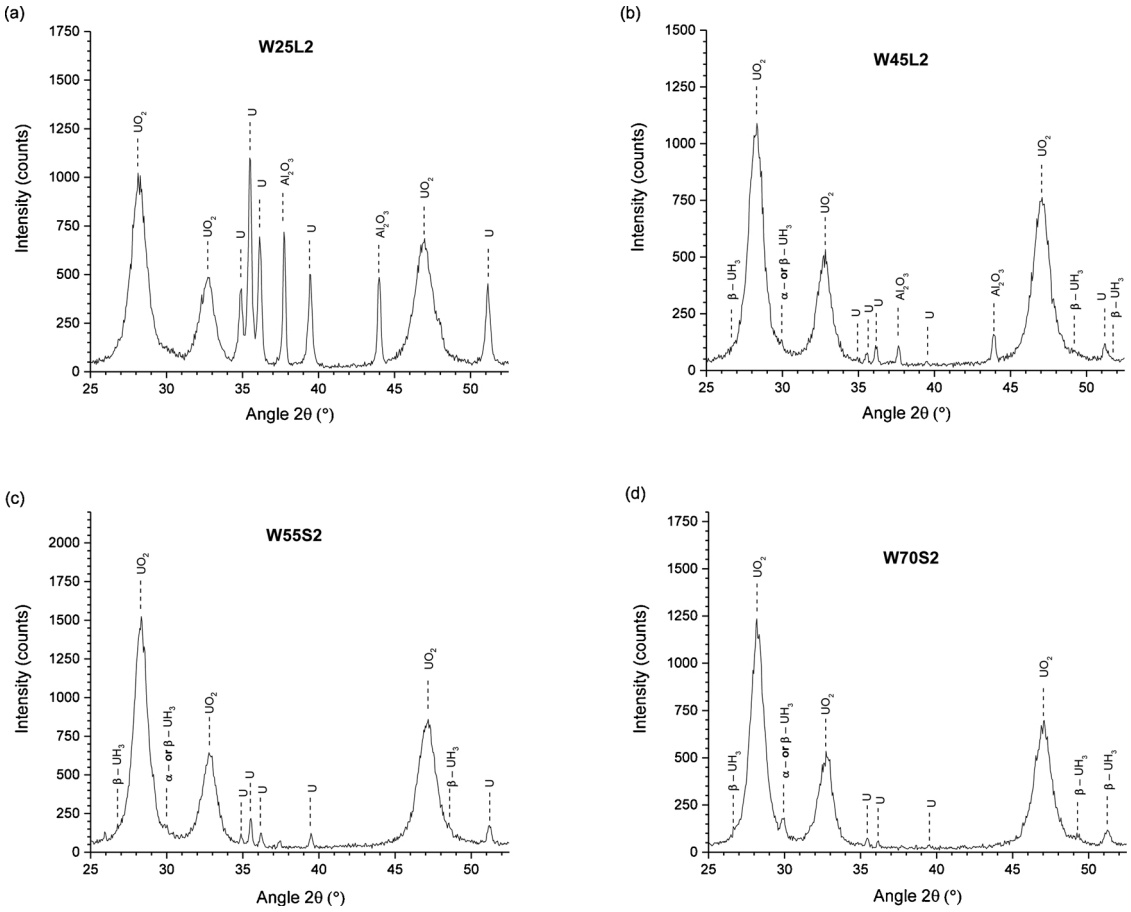

Fig. 8. Raw X-ray diffraction (XRD) spectra for: (a) W25L2; (b)W45L2; (c) W55S2; (d) W70S2 sample. The analyses were performed with a Cu-Kα source at 8 keV, between 25 and 52.5° angle 2θ, 0.05 step and 5 s dwell time.
Figure reproduced from [33].

phase (Fig. 8b and d). For W55S2 only the first three UH_3 peaks could be identified. At ~30° 2-theta (θ), the α-UH_3 and β-UH_3 phase could co-exist and overlap with each other (Fig. 8b–d). The second most intense UH_3 peak, at ~33.07° 2-theta (θ), was overlapped by the strong UO_2 (200) peak and, thus, could not be observed in the spectra. Except for sample W25L2, all were heavily oxidised on their surfaces, exhibiting very strong UO_2 peaks and very weak uranium peaks. Since UH_3 forms at or near the metal-oxide interface, peaks assigned to hydride formation were also found to be very weak in intensity. UH_3-assigned peaks were more easily observable for sample W70S2 which implied that the UH_3 quantity relative to UO_2 was greater on that sample. For sample W25L2, no peaks ascribed to UH_3 have been observed in the spectra (Fig. 8a). However, it is worth noting that for this sample a significant amount of oxide has been detached from the surface leaving the surface close to the metal-oxide interface exposed to air. It is possible that any UH_3 (if formed) could have reacted with air to convert to UO_2. However, this is not considered very likely since UH_3 would have persisted even after partial oxidation [45,46]. Additionally, it is possible that XRD may not have detected the UH_3 phase, if in very small amounts or if in an amorphous phase. No $UO_3{\cdot}H_2O_{(s)}$ was found to form on the samples, which established that H_2 could be evolved on heating samples to the decomposition temperature of UH_3 (250–450 °C) [16]. This information was important for the decomposition analysis presented in the following section.

3.6. TPD - RGA analysis

SIMS and XRD analysis provided direct information about the products generated through corrosion on each sample. However, for both methods, there was a risk of 'missing' hydride that had formed formation.

Thermal desorption combined with analysis of the evolved gases allowed us to indirectly identify if hydride formation had occurred in the systems. RGA analysis allowed verification of the gases generated for several decomposition steps. The thermal cycle applied to the samples involved a constant temperature increase with a stepped ramp rate of (5 °C min^{-1}) and including the following stages:

Step 1: An initial temperature increase to $120 \leq T \leq 150$ °C for ~17 h under continual vacuum. This was considered sufficient time for each sample to release water, hydroxyl, CO, etc. entities from the near surface. Physi- and chemisorbed waters (with associated phases) were considered to be removed by this initial thermal step.

Step 2: Temperature increase to ~220 °C under static vacuum. The working volume was then isolated from the vacuum pumping system to observe any subsequent pressure increase with heating and ensure that no other gases are released close to the lower temperature limit of UH_3 decomposition (~250 °C). In some cases, the gas profile showed further release, with gas analysis resolving a mixture of various gases. H_2, H_2O and OH^- were the dominating entities at this stage. In almost all cases at that stage, H_2 constituted of ≤25% of the overall gas. The temperature was kept constant until no more pressure increase was observed and the volume was quickly evacuated to 1×10^{-7} mbar and then isolated again.

Step 3: A final temperature increase of the system to 360–440 °C was then applied. RGA analysis at this stage yielded ~100% H_2 in the gas phase, indicating that hydride was the predominant compound contributing (via decomposition) to the arising gas in this temperature regime. When no further pressure increase was observed in the system

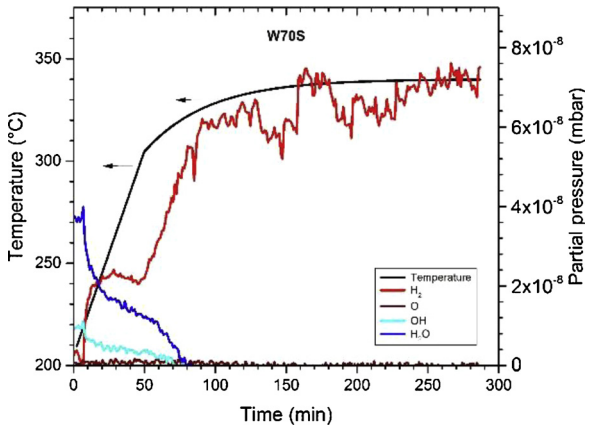

Fig. 9. Residual gas analysis (RGA) profile of the evolved gases for decomposition of reacted uranium (W70S) between.200–450 °C.
Figure reproduced from [33].

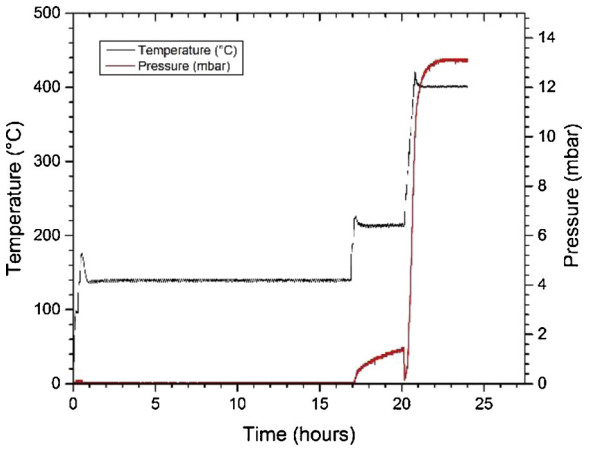

Fig. 10. Pressure and temperature vs. time plot from the thermal process (sample degassing) of W70S2 sample. Pressure increase due to H2 generation is predominantly occurring when temperature is increased above 220 °C. Hydrogen generation at this stage is ascribed to UH3 decomposition.
Figure reproduced from [33].

(complete hydride decomposition), the furnace was switched off and the cell was left to cool down while being pumped. Pumping at this stage ensured removal of hydrogen and re-hydriding prevention on cooling.

Residual analysis of the evolved gases was only conducted for samples W45S, W55S, W70S and a reference polished-U sample. Fig. 9 illustrates an example profile (W70S) of the emerging gases in partial pressure, with increasing temperature, over time, for step 3 of the thermal process.

The gas profile behaviour of a reference polished sample looked very similar to the reacted samples except that all other gas profiles reached background values earlier (~45 min) and no notable H_2 evolution at high temperatures. By also monitoring the cell pressure over the course of the thermal process, it was evident that for all profiles there was negligible pressure increase in the cell, until the point where H_2 became dominant in the gas profile mixture. This time period was also similar to the required time for the temperature to stabilise at the desired value. After that point, only hydrogen was generated and its profile dominated the system (Fig. 9). The pressure in the headspace increased significantly reaching 8.2, 8.9 and 10.75 mbar for W45S, W55S and W70S, respectively. For the non-reacted and polished-U sample, the pressure in the same volume plateaued at 2.1 mbar. That amount was ascribed to stored hydrogen in the bulk of the metal through the fabrication process and, thus, was related to the weight of the sample. Multiple thermal processes were performed for non-reacted and polished samples with the average amount of generated H_2 in the volume, and in relation to the weight, being used as a reference point for our subsequent experiments. Taking into account that all four samples had very similar masses and surface area, we are able to presume that this significant difference in H_2 gas pressure was due to thermal decomposition of UH_3 formed from water corrosion.

After establishing that only H_2 is degassed during the final stage of the thermal process, it was decided not to proceed to analysis of the emerging gases for the remaining samples. Hence, pressure-temperature profiles were derived over the course of the thermal process for all remaining systems. Fig. 10 illustrates an example P–T profile for the W70S2 sample. Contrary to the sample profiles similar to that of Fig. 9, steps 1–3 of the thermal decomposition process were included in Fig. 10.

From the recorded profiles, it is evident that all samples released significant amounts of H_2 when the temperature was raised to ≥220 °C (step 3 of the thermal process), indicating UH_3 decomposition. A limited amount of gas was produced when the samples reached temperatures between 200 and 220 °C (step 2 of the thermal process – Fig. 10). RGA analyses on samples W45S, W55S and W70S showed that this pressure (at step 2) is a mixture of various gases dominated by H_2O, OH^- and H_2. Hydrogen at stage 2 could evolve from recombination of H^+, chemisorbed in the metal-oxide interface or diluted in the oxide layer. Additionally, hydrogen could also originate from water decomposition on the oxide surface [16]. However, it is very possible that limited decomposition of UH_3 had started to occur at this stage, releasing H_2 gas into the free volume. These quantities were not included in our measurements. After full decomposition was achieved for each system, no further pressure increase was observed, and the profile line plateaued.

To quantify the amount of UH_3 produced from each corrosion reaction, the observed pressure change in the headspace at stage 3 of the thermal decomposition process was converted to moles of H_2. This was then converted to moles of UH_3, according to Eq. (2). However, hydrogen was generated at this stage from the disintegration of three possible sources of hydride:

1. **Stored UH_3preserved from the fabrication process.** This type of hydride resides in the bulk of the metal and, according to Danon et al. [16], it decomposes at ≥ 500 °C. Here, the reference samples, which were non-reacted but mechanically polished, released small quantities of H_2 at ~405 - 450 °C.
2. **Interfacial hydride forming as a very thin layer at the metal-oxide interface.** The existence of this hydride was recently confirmed by Martin et al. [27] using APT. This layer has formed through corrosion of uranium in oxygen-free water vapour environments and its thickness was measured at ~5 nm, on average. Inter-layer hydride formation may be regarded to be harmless since it works as a reaction front of constant thickness consuming the metal, while forming more UO_2. It also constitutes a very tiny mass of H_2 in the sample.
3. **Bulk-hydride formation.** This is considered the most 'harmful' type of hydride, which is generated in a blister-like form, on site-specific locations, at the metal-oxide interface, growing vertically and laterally.

Fig. 11 provides a schematic illustrating all three types of hydride. Here, we are interested in measuring the amount of bulk-hydride, which could affect the coherence of the protective oxide layer forming on top, leading to direct exposure of the metal and hydride to air/water.

Quantifications of bulk UH_3 formed were achieved by correcting for 'stored' hydride (via the reference samples) and for 'interfacial' hydride by assigning an average thickness of 5 nm to this type of hydride, as shown in [27], and converting this thickness to a volume of UH_3, using

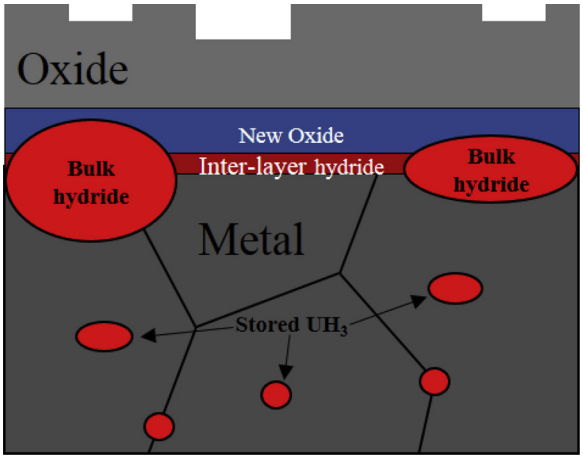

Fig. 11. Types of hydrides present on water-corroded natural uranium metal under contained conditions.
Figure reproduced from [33].

the surface area from each sample. The molar mass of 'interfacial' hydride could then be calculated. Hence, the mass of bulk-hydride (type 3) for each system could be calculated as follows:

$$n_{bulk\ UH_3} = n_{overall\ UH_3} - n_{stored\ UH_3} - n_{inter-layer\ UH_3} \quad (4)$$

For each sample, the amount of bulk hydride (in moles) formed through the reaction was compared to the overall amount of reaction products generated in the solid phase. Since UH_3 formation has been verified and quantified, it is assumed that only UO_2 and UH_3 are generated in the solid phase, through Eqs. (1) and (2) respectively. Table 5 consolidates the results from all samples.

From the analyses, it can be seen that the relative percentage of bulk hydride present in the solid reaction products increases with decreasing reaction temperature. Of course, the total amount of UO_2 (in moles) on the samples reacted at higher temperatures is considerably higher, owing to faster oxidation kinetics. Samples reacted at 45 °C exhibited very comparable UH_3 percentages in the solid phase. The amount of UH_3 on sample W55S2 was potentially underestimated owing to possible H_2 gas mass loss in the system through the thermal decomposition cycle. Thus, this percentage value is excluded from comparison of the 55 °C reacted samples. Interestingly, there is a considerable difference between samples W55S and W55 L, which could imply potential relation of the UH_3 percentage with reaction time. W70S2 sample exhibited a higher percentage of UH_3 in comparison to W70S.

4. Discussion & conclusions

The combined data indicates that bulk UH_3 is produced under the reaction conditions tested (water-immersed samples in sealed conditions). The analyses also showed that the water-formed UH_3 starts to decompose between 225 and 275 °C. Danon et al. [16] measured this temperature as ≥ 250 °C for heavily oxidised samples in air at 25 °C. Thus, our results are in very good agreement with Danon et al. [57]. In stage 2 of the thermal analysis cycle (200–220 °C), a measurable amount of gas was released from the samples. This gas, according to RGA, consisted mainly of H_2O, OH^-, CO_2 and H_2. It is possible, at this stage, for hydrogen to form from partial recombination of H^+ on the surface, which originate from decomposition of water [16].

From Table 5, it was found that even though the absolute masses of UH_3 formed were higher on the higher temperature samples, the ratios of UH_3 percentage to overall solid corrosion products were lower. It is believed that the more rapid oxidation kinetics at higher temperature leads to a more substantial loss of coherence in the oxide layer leading to more extensive exposure of the UH_3 to direct oxidation by water, through Eq. (5):

$$2UH_{3(s)} + 4H_2O_{(l)} \rightarrow 2UO_{2(s)} + 7H_{2(g)} \quad (5)$$

On the other hand, from physical observation of the samples reacted at lower temperatures, the oxide was less flaky, less porous and better adhered to the surface. This would result in limited diffusion pathways for liquid water to reach the metal-oxide interface. Thus, any UH_3, if formed, is better protected from oxidation, in comparison to the higher temperature samples.

We confirmed that both of Eqs. (1) and (2) will occur under these conditions. Eq. (1), that produces $UO_{2(s)}$ and $H_{2(g)}$, will precede and, after H_2 builds up in pressure in the vicinity of the metal, Eq. (2) will follow to produce $UH_{3(s)}$ [9,16,18,47,48]. The rates of the reaction were found to be considerably slower in comparison to the literature. This is justified by the existence of a second reaction process (Eq. (2)), which withholds/consumes the oxidation-generated H^+ ions to form UH_3, thus leading to underestimation of the rate. This is also evidenced by the considerable difference between the corrosion rates derived from H_2 gas generation method vs average corrosion layer thickness derivations (Table 3). The activation energy (E_α) was calculated through Eq. (3) at ~50 kJ mole^{-1}. In the literature, the E_α reported were slightly higher, with the values ranging from 53.1–64.9 kJ mole^{-1}, for similar reaction conditions [41,49–52]. The reaction rates (Fig. 3) derived from H_2 gas generation, if not yielding a quasi-constant slope (constant rate), were seen to switch to slower reaction rate regimes (smaller slope) over the course of time (Fig. 3). At this point, hydrogen gas generation is decelerated and, since Eq. (2) will absorb/consume H_2 and will occur at a later stage, it is logical to assume that UH_3 formation definitely occurs (if not commences) at this stage of the reaction process. It is suggested that at a certain stage two processes may occur separately or simultaneously in the system: (a) hydrogen gas generation will start being suppressed by the headspace pressure; and/or (b) hydrogen gas exchange between the water and the headspace gas of the free volume. Of course, for process (b) to occur, interaction between water and headspace gas should take place. It is unclear at this stage which of the

Table 5
Bulk-hydride quantification for all reaction samples. The percentage ratio of UH_3 to overall solid reaction products was also calculated.

Sample	Reaction time (hours)	Working volume* (cm^3)	Final T of decomposition (K)	Pressure increase due to UH_3 decomposition (mbar)	mmol of interlayer hydride (for avg. thickness of 5 nm)	mmol of bulk UH_3 (Eq. 4)	mmol of UO_2 (derived from Eq.1)	Percentage ratio of UH_3 to overall solid corrosion products (assuming only UO_2 and UH_3 are produced) (%)
W45S	126	108.2	632.8	8.2	8.2E-05	0.009	0.05	14.6
W45L	1621.6	213.3	638.6	20.9	4.4E-05	0.055	0.28	16.34
W45L2	1046	212.8	671	7.2	3.8E-05	0.017	0.07	19.61
W55S	345	108.3	626.7	8.9	8.1E-05	0.001	0.08	10.71
W55S2	397.2	212.9	672.1	1.9	4.1E-05	0.004	0.24	1.56[a]
W55L	1618.2	213.3	676.3	11.3	4.6E-05	0.03	0.85	3.13
W70S	329	108.2	613	10.8	8.7E-05	0.01	0.62	1.97
W70S2	436.3	213.2	673.1	13.2	8.3E-05	0.03	0.67	4.43

[a] Potential underestimation of this value owing to possible H_2 gas loss through the decomposition process.

above processes (if not both) leads to the observed deceleration of H_2 evolution. It is believed that process (a) is more likely to occur, driven by an equalisation of hydrogen concentration throughout the oxide thickness and into the water. Similarly, if hydrogen migrated from the gas phase into the water and reached the oxide surface, chemisorbed water and/or hydrogen already generated at the oxide-metal interface would inhibit hydrogen chemisorption and dissociation, by accommodating all available sorption sites [53]. Still, both processes would result in H_2 build-up in the vicinity of the metal and, thus, potential to form UH_3. Baker et al. [54] found the rate of uranium corrosion with liquid water (through H_2 evolution) to be approximately halved when ~71–2027 mbar of CO_2 were introduced to the headspace volume. The quantity of CO_2 in the headspace remained unchanged, while no carbon monoxide was detected in the course of the reaction. It was suggested that CO_2 is absorbed on the oxide surface as carbonate ions which block H_2 evolution in the gas phase. On the same study, 1013.25 mbar (101,325 Pa) of N_2 and 6080 mbar (607,950 Pa) of H_2 were used as headspace gases, in separate experiments, with no significant changes observed in the rate or the reaction products of the system [54]. However, these experiments were conducted in an enclosed system which was periodically opened for thermogravimetric analysis to take place and, thus, the headspace pressure effect was only observed for a limited time period. Additionally, in that work, there is limited (if not at all) information about the headspace volume, mass of sample and volume of water of the ternary system, which could be very different from this work. However, UH_3 formation was also evidenced in that work [54]. Gas suppression or headspace gas/water interaction are expected to eventually lead to UH_3 formation since the generated hydrogen is not fully released in the gas phase, but remains in the vicinity of the metal. It is considered that there is no significant difference between the time periods where H_2 gas suppression and/or interaction occurs vs. UH_3 formation. In this work, we assume that these two processes occur almost simultaneously in the system. In the reaction systems where this switch to slower H_2 gas generation was observed, the threshold pressure, signifying UH_3 formation, was recorded. Table 6 integrates the threshold pressures for each system.

From Table 6 it can be seen that the liquid water volume in relation to the mass of the samples is low. This could possibly play a key role in the formation of UH_3 in the system, even though the samples were fully immersed in the water. Except for W55S, which generally exhibited different behaviour and had a very low 'threshold' pressure of 187.4 mbar, all other samples exhibited a comparable 'threshold' pressure in the 500-mbar range. Thus, it may be assumed that in an extreme scenario where significant mass of uranium is contained in a water (or water-starved) environment, with gas pressures in the 0.5 bar range, UH_3 is expected to form as part of the gas suppression and/or equilibrium gas/water exchange process. This is a highly critical finding for the short-term complex disposal of ILW in fuel ponds and silos.

However, observing UH_3 formation also in the other systems (where gas generation did not show this slope-switch) indicates that these processes are not compulsory for UH_3 formation to occur on the sample. One additional parameter that could facilitate UH_3 generation in the system was positioning of the samples inside the ceramic crucible containing the water. Part of the hydrogen generated by oxidation of the uranium surface facing down (bottom of the crucible) could stay trapped and in the vicinity of the sample. With continuous H_2 production and build-up in these enclosed areas, UH_3 could be inevitable in the system. Trapped H_2 is considered a highly probable scenario in numerous waste storage scenarios, specifically for uranium-rich Magnox cladding, where hydrogen generated from Magnox corrosion contribute significantly to UH_3 formation.

Table 6
Threshold headspace pressures for UH_3 formation for samples W55S, W55 L, W70S and W70S2.

Sample	Sample mass (g)	Volume of water (ml)	Working volume (cm^3)	Threshold pressure (mbar)[a]
W55S	4.79	4	84.6	187
W55L	2.12	4	84.8	541
W70S	5.35	4	180.1	435
W70S2	4.53	4	84.6	559

[a] The headspace pressure includes all generated agents in the gas phase, mainly H_2 and H_2O vapour.

From the analysis, it is suggested that, for an enclosed system of the above-mentioned parameters, there is a threshold headspace pressure in the range of 500 mbar (Table 6) over which (a) H_2 gas suppression or (b) liquid water-H_2 gas exchange occurs. This pressure includes the pressure of water vapour saturation at the temperature of the reaction, which for 55 °C and 70 °C is 157 and 311 mbar, respectively. Thus, the pressures of H_2 needed for this phenomenon to occur were significantly low. Both these processes (a & b) would lead to increased hydrogen concentration in the vicinity of the metal and, thus potential UH_3 formation. It is unclear at this stage which one (if not both) of these processes takes place in the system above this threshold pressure.

To summarize, the low-temperature corrosion reaction of uranium with liquid water was investigated under immersed and sealed conditions with an initially evacuated headspace volume. Ten samples were examined under four different temperatures (25, 45, 55 and 70 °C), and after varying reaction times. The rate of corrosion was derived by monitoring the pressure changes in the reaction cell as a function of time (ascribed to H_2 generation from U corrosion). Post-corrosion examination of the uranium surfaces was conducted using FIB, SIMS and XRD. Measurements of water pH were made immediately after the experiments were halted. As a final analysis step, the samples were degassed under a three-step thermal process to induce UH_3 decomposition and verify the mass of hydride that had formed during corrosion. RGA analysis of the desorbed gases was performed for the first set of samples, while P–T analyses over time were conducted for the remaining samples. From the analyses, it was concluded that:

i Bulk-UH_3 forms at the metal-oxide interface, on the majority of the samples.
ii Lower temperature reaction conditions yielded higher UH_3 proportions in the solid corrosion products. However, the absolute UH_3 quantities are markedly higher on the higher temperature samples.
iii The rates of corrosion were calculated based on recorded H_2 evolution and were found to be considerably slower in comparison to the literature.
iv From plotting the rates derived from the gas generation method, the activation energy (E_α) of the oxidation reaction (Eq. (1)) was measured at 50 kJ $mole^{-1}$.
v Examining the pressure evolution plots at the later stages of the reaction process, where pressure build-up is considerable in the headspace, a notable switch to a lower rate of gas evolution was observed. By combining this behaviour with the post-examination analyses, it was confirmed that there is a critical 'threshold' headspace pressure ~0.5 bar over which pressure deficiency is observed in the free headspace. It is suggested that bulk-UH_3 formation is facilitated if not accelerated by this process. The mechanism under which this process occurs remains unknown.

In future work, the process under which gas generation deceleration occurs in the free headspace will be addressed. This will be done by introducing isotopically-labelled D_2 of known pressure to the headspace volume and, thus, start observing the reaction from a later stage where gas build-up is already present on the system. Pressurisation of the free volume from the initial stages will also facilitate in verifying if these processes leading to H_2 evolution deceleration occur immediately in the system by deliberately using headspace pressures below, at and over the observed 'threshold' pressure. Additionally, post-examination of the surfaces will elucidate as to whether 'deuterated' hydride forms in the

sample. This could provide more insight into the occurring processes and will facilitate in understanding the mechanism of this ternary reaction system.

Acknowledgements

The authors would like to thank the Engineering and Physical Sciences Research Council (EPSRC) and Sellafield Ltd for funding this project as part of 42-month PhD research studentship (Ref: 1338575), at the Interface Analysis Centre (IAC), School of Physics, University of Bristol. We would also like to thank Mr John Jowsey and Dr Anna Adamska from the Sellafield Centre for Expertise in Uranium and Reactive Metals (URM) for contextual guidance and technical input.

References

[1] Sellafield Plan, (2011) Cumbria www.sellafieldsites.com.
[2] Nuclear decommissioning authority (NDA), Radioactive Wastes in the UK: A Summary of the 2013 Inventory, Nuclear decommissioning authority (NDA), Cumbria, 2014.
[3] ILW Treatment and Storage, (2013) Cumbria www.sellafieldsites.com.
[4] Pile Fuel Storage Pond, Sellafield Ltd, Cumbria, 2013www.sellafieldsites.com.
[5] J. Frank, A. Roebuck, Crevice Corrosion of Uranium and Uranium Alloys, Argonne National Laboratory, (ANL -5380), Lemont, Illinois, 1955.
[6] J. Draley, W. Ruther, Some unusual effects of hydrogen in corrosion reactions, J. Electrochem. Soc. 104 (1957) 329–333.
[7] B. Hopkinson, Kinetics of the uranium-steam reaction, J. Electrochem. Soc. 106 (1959) 102–106.
[8] T. Kondo, E. Verink, F. Beck, M. Fontana, Gas chromatographic and gravimetric studies of uranium oxidation mechanism, Corrosion 20 (1964) 314t–320t.
[9] M.M. Baker, L. Less, S. Orman, Uranium + water reaction. Part 1.- Kinetics, products and mechanism, Trans. Faraday Soc. 62 (1966) 2513–2524.
[10] T. Kondo, F. Beck, M. Fontana, A gas chromatographic study on the kinetics of uranium oxidation in moist environments, Corrosion 30 (1974) 330–341.
[11] M. Bennett, B. Myatt, D. Silvester, J. Antill, The oxidation behaviour of uranium in air at 50–300 °C, J. Nucl. Mater. 57 (1975) 221–236.
[12] K. Winer, C. Colmenares, R. Smith, F. Wooten, Interaction of water vapour with clean and oxygen-covered uranium surfaces, Surf. Sci. 183 (1987) 67–99.
[13] S.C. Marschman, T. Pyecha, J. Abrefah, Metallographic Examination of Damaged N Reactor Spent Nuclear Fuel Element SFEC5, 4378, Pacific Northwest Laboratory, Richland, WA (United States), 1997.
[14] J. Abrefah, R.L. Sell, Oxidation of K-West Basin Spent Nuclear Fuel in Moist Helium Atmosphere, Pacific Northwest National Laboratory, Richland, WA (US), 1999.
[15] T.C. Totemeier, R.G. Pahl, S.M. Frank, Oxidation kinetics of hydride-bearing uranium metal corrosion products, J. Nucl. Mater. 265 (1999) 308–320.
[16] A. Danon, J. Koresh, M. Mintz, Temperature programmed desorption characterization of oxidized uranium surfaces: relation to some gas-uranium reactions, Langmuir 15 (1999) 5913–5920.
[17] C.H. Delegard, A.J. Schmidt, Uranium Metal Reaction Behaviour in Water, Sludge, and Grout Matrices, Pacific Northwest National Laboratory, 2008.
[18] J. Waber, A Review of the Corrosion Behaviour of Uranium, Los Alamos Scientific Laboratory, New Mexico, 1956.
[19] C. Colmenares, R. Howell, T. McCreary, Oxidation of Uranium Studied by Gravimetric and Positron Annihilation Techniques, Lawrence Livermore National Laboratory, CA (USA), 1981.
[20] J.M. Haschke, Reactions of Plutonium and Uranium With Water: Kinetics and Potential Hazards, Los Alamos National Laboratory, 1995.
[21] M. Kaminski, Batch Tests with Unirradiated Uranium Metal Fuel Program Report, Argonne National Laboratory, Illinois (USA), 2002.
[22] C. Stitt, C. Paraskevoulakos, N. Harker, A. Banos, K. Hallam, C. Jones, T. Scott, Real-time, in-situ deuteriding of uranium encapsulated in grout; effects of temperature on the uranium-deuterium reaction, Corros. Sci. 127 (2017) 270–279.
[23] C. Stitt, C. Paraskevoulakos, A. Banos, N. Harker, K. Hallam, A. Davenport, S. Street, T. Scott, In-situ, time-resolved monitoring of uranium in BFS: OPC grout. Part 1: corrosion in water vapour, Sci. Rep. 7 (2017).
[24] J. Jowsey, Personal Communication (2016).
[25] F. Le Guyadec, X. Génin, J. Bayle, O. Dugne, A. Duhart-Barone, C. Ablitzer, Pyrophoric behaviour of uranium hydride and uranium powders, J. Nucl. Mater. 396 (2010) 294–302.
[26] C. Ablitzer, F. Le Guyadec, J. Raynal, X. Génin, A. Duhart-Barone, Influence of superficial oxidation on the pyrophoric behaviour of uranium hydride and uranium powders in air, J. Nucl. Mater. 432 (2013) 135–145.
[27] T. Martin, C. Coe, P. Bagot, P. Morrall, G.W. Smith, T. Scott, M. Moody, Atomic-scale studies of uranium oxidation and corrosion by water vapour, Sci. Rep. 6 (2016).
[28] A. Banos, C.P. Jones, T.B. Scott, The effect of work-hardening and thermal annealing on the early stages of the uranium-hydrogen corrosion reaction, Corros. Sci. 131 (2018) 147–155.
[29] A. Banos, C. Stitt, T. Scott, The effect of sample preparation on uranium hydriding, Corros. Sci. 113 (2016) 91–103.
[30] A. Banos, T.B. Scott, Statistical analysis of UH_3 initiation using electron back-scattered diffraction (EBSD), Solid State Ionics 296 (2016) 137–145.
[31] R. Asuvathraman, S. Rajagopalan, K. Ananthasivan, C. Mathews, R. Mallya, Surface studies on uranium monocarbide using XPS and SIMS, J. Nucl. Mater. 224 (1995) 25–30.
[32] F. Weigel, J. Katz, G. Seaborg, J.J. Katz, G.T. Seaborg, L.R. Morss (Eds.), The Chemistry of the Actinide Elements, vol. 1, 1986, p. 361 Chapmann and Hall, London.
[33] A. Banos, Investigation of Uranium Corrosion Under Mixed Water-Hydrogen Environments, PhD thesis School of Physics, University of Bristol, Bristol (UK), 2017.
[34] C.P. Jones, T.B. Scott, J.R. Petherbridge, J. Glascott, A surface science study of the initial stages of hydrogen corrosion on uranium metal and the role played by grain microstructure, Solid State Ionics 231 (2013) 81–86.
[35] A. Schürenkämper, Kinetic studies of the hydrolysis of uranium monocarbide in the temperature range 30 °C–90 °C, J. Inorg. Nucl. Chem. 32 (1970) 417–429.
[36] R. Dell, V. Wheeler, N. Bridger, Hydrolysis of uranium mononitride, Trans. Faraday Soc. 63 (1967) 1286–1294.
[37] G.R. Rao, S. Mukerjee, V. Vaidya, V. Venugopal, D. Sood, Oxidation and hydrolysis kinetic studies on UN, J. Nucl. Mater. 185 (1991) 231–241.
[38] T. Scott, J. Petherbridge, N. Harker, R.J. Ball, P. Heard, J. Glascott, G. Allen, The oxidative corrosion of carbide inclusions at the surface of uranium metal during exposure to water vapour, J. Hazard. Mater. 195 (2011) 115–123.
[39] C. Staff, Deviations from the Ideal Gas Law, Chemical Education Digital Library, 2010.
[40] A. Praga, A. Pajunen, MCO Loading and Cask Loadout Technical Manual, (1998).
[41] S. Orman, Uranium Compatibility Studies 1: Interaction of Uranium with Gas-Free Water and Water Vapor, Report AWRE-094/63, Atomic Weapons Research Establishment, Aldermaston, England, 1963.
[42] J. Bloch, F. Simca, M. Kroup, A. Stern, D. Shmariahu, M. Mintz, Z. Hadari, The initial kinetics of uranium hydride formation studied by a hot-stage microscope technique, J. Less Common Met. 103 (1984) 163–171.
[43] L. Owen, R. Scudamore, A microscope study of the initiation of the hydrogen-uranium reaction, Corros. Sci. 6 (1966) 461–468.
[44] T.C. Totemeier, A Review of the Corrosion and Pyrophoricity Behavior of Uranium and Plutonium, Government Research Announcements and Index 45, USA), 1995.
[45] P. Morrall, D. Price, A. Nelson, W. Siekhaus, E. Nelson, K. Wu, M. Stratman, W. McLean, ToF-SIMS characterization of uranium hydride, Philos. Mag. Lett. 87 (2007) 541–547.
[46] C. Stitt, N. Harker, K. Hallam, C. Paraskevoulakos, A. Banos, S. Rennie, J. Jowsey, T. Scott, An investigation on the persistence of uranium hydride during storage of simulant nuclear waste packages, PLoS One 10 (2015) e0132284.
[47] G.C. Allen, P.M. Tucker, R.A. Lewis, X-ray photoelectron spectroscopy study of the initial oxidation of uranium metal in oxygen + water-vapour mixtures, J. Chem. Soc. Faraday Trans. 2: Mol. Chem. Phys. 80 (1984) 991–1000.
[48] C. Colmenares, Oxidation mechanisms and catalytic properties of the actinides, Prog. Solid State Chem. 15 (1984) 257–364.
[49] J.M. Haschke, Corrosion of uranium in air and water vapor: consequences for environmental dispersal, J. Alloys Compd. 278 (1998) 149–160.
[50] A. Ritchie, A review of the rates of reaction of uranium with oxygen and water vapour at temperatures up to 300 °C, J. Nucl. Mater. 102 (1981) 170–182.
[51] A. Ritchie, The kinetics and mechanism of the uranium-water vapour reaction—an evaluation of some published work, J. Nucl. Mater. 120 (1984) 143–153.
[52] A. Ritchie, R. Greenwood, S. Randles, D. Netherton, M.J. Whitehorn, Measurements of the rate of the uranium-water vapour reaction, J. Nucl. Mater. 140 (1986) 197–201.
[53] E. Tiferet, M. Mintz, I. Jacob, N. Shamir, Inhibition of hydrogen chemisorption on uranium surfaces by traces of water vapor, Surf. Sci. 601 (2007) 4925–4930.
[54] M.M. Baker, L. Less, S. Orman, Uranium + water reaction. Part 2.- effect of oxygen and other gases, Trans. Faraday Soc. 62 (1966) 2525–2530.